Taylor & Francis
Taylor & Francis Group

Synthesis, crystal structure, redox behavior and DNA-binding properties of a series of copper(II) complexes with two new carboxamide derivatives

Biplab Mondal, Buddhadeb Sen, Abhishek Maji, Ennio Zangrando & Pabitra Chattopadhyay

⊞ View supplementary material ⧉

🗓 Accepted author version posted online: 14 Aug 2015.
Published online: 16 Sep 2015.

✎ Submit your article to this journal ⧉

📊 Article views: 94

🔍 View related articles ⧉

⬙ View Crossmark data ⧉

Taylor & Francis
Taylor & Francis Group

Synthesis, crystal structure, redox behavior and DNA-binding properties of a series of copper(II) complexes with two new carboxamide derivatives

BIPLAB MONDAL†, BUDDHADEB SEN†, ABHISHEK MAJI†,
ENNIO ZANGRANDO‡ and PABITRA CHATTOPADHYAY*†

†Department of Chemistry, Burdwan University, Burdwan, India
‡Department of Chemical and Pharmaceutical Sciences, Trieste, Italy
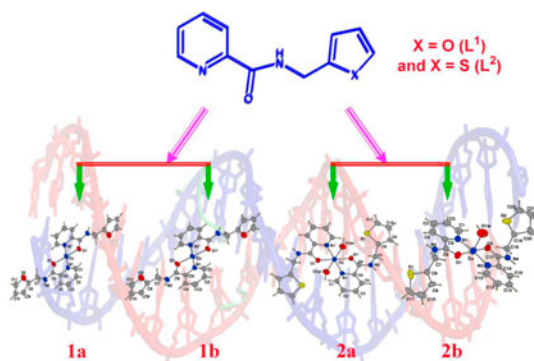
Four mononuclear copper(II) complexes of two new carboxamide derivatives formulated as [Cu(L^1)$_2$](ClO$_4$)$_2$ (**1a**), [Cu(L^1)$_2$](NO$_3$)$_2$ (**1b**), [Cu(L^2)$_2$(H$_2$O)$_2$](ClO$_4$)$_2$ (**2a**), and [Cu(L^2)$_2$(H$_2$O)](NO$_3$)$_2$ (**2b**) have been isolated in pure form from the reaction of L^1 and L^2 [where L^1 = *N*-(furan-2-yl-methyl)-2-pyridinecarboxamide and L^2 = *N*-(thiophen-2-ylmethyl)-2-pyridinecarboxamide] with copper(II) salts of perchlorate and nitrate. All the complexes were characterized by physicochemical and spectroscopic tools along with single-crystal X-ray diffraction studies. The structural analyses showed that **1** is monomeric of square planar geometry with copper(II) chelated by two L^1 ligands. Complex **2** differs in coordination geometry, being octahedral and distorted square pyramidal. Two L^2 ligands occupy the equatorial positions of the octahedral **2a** and the basal sites of the pyramidal **2b**, with water molecules that complete the coordination sphere in each case. Electrochemical studies using cyclic voltammetry showed a reversible redox behavior of the copper(II) in **1** and **2**. The electronic spectroscopic behavior and the trend of one electron equivalent redox potential corresponding to a Cu^{II}/Cu^{I} couple have also been confirmed by density functional theory calculations. The spectroscopic and viscosity measurement study in tris–HCl buffer suggested an intercalative interaction of **1a** and **2** with calf thymus DNA likely due to the stacking between the non-coordinated furan and thiophene chromophore with the base pairs of DNA.

Keywords: Copper(II) complex; Crystal structure; Redox behavior; DFT; DNA binding

---

*Corresponding author. Email: pchattopadhyay@chem.buruniv.ac.in

1. Introduction

Coordination chemistry of carboxamide derivatives, especially toward transition metal ions, has attracted attention because pyridine carboxamide complexes are useful in asymmetric catalysis [1, 2], dendrimer preparation [3], molecular receptor synthesis [4], and also for biological applications such as the synthesis of compounds with possible anti-tumor properties [5–8]. Carboxamide [–C(O)NH–], a key moiety of the primary structure of proteins, represents an important ligand in coordination chemistry, since its chelating rigid nature imparts a unique balance of stability *versus* reactivity and allows for developments in catalytic transformations. Copper, third most abundant soft transition metal, plays significant roles in the active sites of a large number of metalloproteins. Specifically, Cu(II)/Cu(I) redox systems take part in different catalytic processes in the human body such as supplying energy for biochemical reactions, cross-links in collagen and elastin, sustaining and repairing connective tissues related to heart and arteries, and controlling of oxidative stress and disorders associated with neurodegenerative diseases. The structural and reactivity studies of copper(II) complexes with ligands including a carboxamide [–C(O)NH–]could provide useful insight into the chemistry and biochemistry of bioactive molecules.

Studies on copper(II) complexes with DNA have attracted considerable interest because of the ability of these complexes to bind to and cleave the double helix [9–12]. DNA can provide a range of binding sites and different covalent and non-covalent interactions such as intercalation, groove binding, electrostatic binding, and hydrogen bonds with metal complexes, and from pharmacological mechanistic studies, it is well-known that intercalation is one of the most important of these interactions. Therefore, the search for drugs showing intercalative binding properties to DNA has been an active research area [13–16].

In continuation of our interest on the interaction of metal complexes of nitrogen/oxygen ligands with calf thymus DNA (CT-DNA) [17–21], herein we report an account of the synthesis, structural characterization, and DNA-binding study of copper(II) complexes of two ligands, furan-2-ylmethyl-amide (L^1) and thiophen-2-ylmethyl-amide (L^2) derived from pyridine-2-carboxylic acid. The binding constants K_b (derived from UV–vis study) and the quenching constant K_{sv} (obtained from fluorescence displacement experiments using ethidium bromide) have been determined in order to establish the binding mode of these complexes to double helix DNA. The binding affinity of these complexes with calf thymus DNA has also been studied by carrying out viscosity measurements.

2. Experimental

2.1. *Materials*

Reagent grade pyridine-2-carboxylic acid, furfuryl amine, 2-thiophenemethyl amine, Cu(NO$_3$)$_2$·3H$_2$O, and Cu(ClO$_4$)$_2$·6H$_2$O were purchased from Sigma-Aldrich and used as received. CT-DNA, obtained from Bangalore Genei, India, and ethidium bromide (EB) from Sigma was used as received. All other chemicals and solvents were of analytical grade.

2.2. *Physical measurements*

The elemental (C, H, and N) analyses were performed on a Perkin-Elmer model 2400 elemental analyzer. IR spectra of ligands and complexes were recorded on a Perkin-Elmer

FTIR model RX1 spectrometer (KBr disk, 4000–400 cm^{-1}). Room temperature magnetic susceptibility was recorded using a vibrating sample magnetometer PAR 155 model. The electronic absorption spectra were recorded on a JASCO UV–vis/NIR spectrophotometer model V-570. The fluorescence spectra of complexes bound to DNA were obtained at an excitation wavelength of 522 nm with the Fluorimeter Hitachi-4500. Redox potentials were measured using a CHI620D potentiometer in DMF at complex concentration of ~ 10^{-3} mol L^{-1} at 298 K. Viscosity experiments were conducted in an Ostwald's viscometer, immersed in a thermostatic water-bath maintained at 25 °C.

2.3. Synthesis of L^1 and L^2

A common synthetic procedure has been followed to obtain **L^1** and **L^2**. To a pyridine solution of pyridine-2-carboxylic acid (1.231 g, 10 mmol), furfurylamine (0.9712 g, 10 mmol) for **L^1** or 2-thiophenemethyl amine (1.1312 g, 10 mmol) for **L^2** was added with stirring. Then, tri-phenylphosphite (3.101 g, 10 mmol) was added to this mixture and heated in an oil bath at 80 °C for 6 h (scheme 1). The resulting orange solution was allowed to evaporate for a few days to collect a white crystalline solid after washing with methanol and water thoroughly. The crystalline material dried in vacuo over silica gel was used for characterization using physicochemical and spectroscopic tools.

L^1: **C$_{11}$H$_{10}$N$_2$O$_2$**: mp (°C): 99 ± 2. Anal. Found: C, 65.40; H, 4.91; N, 13.92; Calcd: C, 65.34; H, 4.98; N, 13.85. IR (cm^{-1}): $\nu_{C=N}$ 1463, $\nu_{C=O}$ 1660, ν_{N-H} 3344. ^{1}H NMR (δ, ppm in dmso-d$_6$): 8.95 (d, 1H); 8.40–8.19 (m, 2H); 8.05–7.82 (m, 2H); 7.39 (m, 1H); 6.06–6.19 (m, 2H); 4.15 (s, 2H of CH$_2$). Yield: 1.636 g (80–82%).

L^2: **C$_{11}$H$_{10}$N$_2$OS**: mp (°C): 90 ± 2. Anal. Found: C, 60.62; H, 4.58; N, 12.98; Calcd: C, 60.53; H, 4.62; N, 12.83. IR (cm^{-1}): $\nu_{C=N}$, 1462, $\nu_{C=O}$, 1654, ν_{N-H} 3317. ^{1}H NMR (δ, ppm in dmso-d$_6$): 8.91 (d, 1H); 8.40–8.20 (m, 2H); 8.03–7.81 (m, 2H); 6.61–6.93 (m, 3H); 4.17 (s, 2H of CH$_2$).Yield: 1.831 g (82–85%).

2.4. Synthesis of 1 and 2

The complexes were synthesized following a common procedure as described below. The organic compound (2.0 mmol, 404 mg of **L^1**, or 436 mg of **L^2**) was dissolved in dry ethanol by stirring the mixture for 15 min. To this solution, an ethanolic solution of cupric perchlorate hexahydrate (Cu(ClO$_4$)$_2$·6H$_2$O, 373 mg, 1.0 mmol) for **1a** and **2a** or cupric nitrate trihydrate (Cu(NO$_3$)$_2$·3H$_2$O, 249 mg, 1.0 mmol) for **1b** and **2b** was added and stirring continued for a further 4 h (scheme 1). The resulting mixture was filtered, and the clear filtrate was collected. The filtrate was kept at room temperature to reduce the volume of the solution by slow evaporation. The product was collected by washing with cold ethanol and water and dried in vacuo. Pure crystalline product was obtained from ethanol. The crystallized material so obtained was used for elemental analysis and characterization with physicochemical and spectroscopic tools. Single crystals of **1a**, **2a**, **1b**, and **2b** suitable for X-ray diffraction were obtained by slow evaporation of ethanolic solutions.

Complex **1a**: [Cu(L^1)$_2$](ClO$_4$)$_2$: C$_{22}$H$_{20}$N$_4$O$_{12}$CuCl$_2$: Anal. Found: C, 39.54; H, 3.06; N, 8.35; Cu, 9.60; Calcd: C, 39.62; H, 3.02; N, 8.40; Cu, 9.53. IR (cm^{-1}): ν_{NH} 3275, $\nu_{C=N}$ 1469, ν_{ClO4} 1080, 628, $\nu_{C=O}$ 1631. Magnetic moment (μ, B.M.): 1.74. Conductivity (Λ_o, Ohm^{-1} cm^2 mol^{-1}) in MeOH: 194. Yield: 0.40 g (60%).

Complex **1b**: $[Cu(L^1)_2](NO_3)_2$: $C_{22}H_{20}CuN_6O_{10}$: Anal. Found: C, 44.53; H, 3.45; N, 14.21; Cu, 10.68; Calcd: C, 44.59; H, 3.40; N, 14.18; Cu, 10.73. IR (cm^{-1}): ν_{OH}, 3448, ν_{NH} 3221; $\nu_{C=N}$ 1473; ν_{NO3}, 1381; $\nu_{C=O}$ 1631. Magnetic moment (μ, B.M.): 1.73. Conductivity (Λ_o, Ohm^{-1} cm^2 mol^{-1}) in MeOH: 201. Yield: 0.402 g (68%).

Complex **2a**: $[Cu(L^2)_2(H_2O)_2](ClO_4)_2$: $C_{22}H_{24}N_4O_{12}S_2CuCl_2$: Anal. Found: C, 35.87; H, 3.33; N, 7.65; Cu, 8.58; Calcd: C, 35.95; H, 3.29; N, 7.62; Cu, 8.65. IR (cm^{-1}): ν_{NH} 3248, $\nu_{C=N}$ 1469, ν_{ClO4} 1080, 628, $\nu_{C=O}$ 1631. Magnetic moment (μ, B.M.): 1.71. Conductivity (Λ_o, Ohm^{-1} cm^2 mol^{-1}) in MeOH: 184. Yield: 0.514 g (70%).

Complex **2b**: $[Cu(L^2)_2(H_2O)](NO_3)_2 \cdot H_2O$: $C_{22}H_{24}N_6O_{10}S_2Cu$: Anal. Found: C, 39.95; H, 3.61; N, 12.80; Cu, 9.54; Calcd: C, 40.03; H, 3.66; N, 12.73; Cu, 9.63. IR (cm^{-1}): ν_{OH} 3450; ν_{NH} 3223; $\nu_{C=N}$ 1473; ν_{NO3} 1382; $\nu_{C=O}$ 1631. Magnetic moment (μ, B.M.): 1.73. Conductivity (Λ_o, Ohm^{-1}cm^2 mol^{-1}) in MeOH: 204. Yield: 0.42 g (65%).

2.5. *X-ray crystallography*

Crystals of **1** and **2** that resulted from the syntheses were found suitable for structural studies. The X-ray single-crystal diffraction data were collected using Mo-K$_\alpha$ radiation ($\lambda = 0.71073$ Å) on a Bruker Smart Apex II diffractometer equipped with a CCD area detector. Data collection and data reduction were carried out using the Bruker Smart Apex and Bruker Saint packages [22]. The structures were solved by direct methods using SHELXS-97 [23] and refined by full-matrix least squares method based on F^2 using SHELXL-97 [23]. In **2b**, a thiophene was found disordered over two coplanar orientations and $S(2)$ was refined as a mixed S/C species with occupancy 0.484(8)/0.516(8) and *vice versa* for C(20). Hydrogens were fixed in calculated positions except those of water molecules and of amino groups N2 (or N2/N4 in **2b**), which were detected in the electron density map and refined. All non-hydrogen atoms were refined anisotropically. All calculations were performed using the WinGX package [24]. Crystallographic data and details of refinements of **1b**, **2a**, and **2b** are tabulated in table 1. The pattern diffraction of **1a** was of low quality leading to a poor structural model (final R factor = 9.63) and data are included as Supplementary Information.

2.6. *DNA-binding experiments*

The tris–HCl buffer solution (pH 7.2) used in all the CT-DNA experiments was prepared using deionized and sonicated HPLC grade water (Merck). The CT-DNA used in the experiments was sufficiently free from protein as the ratio of UV absorbance of DNA solution in tris–HCl at 260 and 280 nm (A_{260}/A_{280}) was 1.9 [25]. The concentration of DNA was estimated using the extinction coefficient (6600 M^{-1} cm^{-1}) at 261 nm, [26] and the stock solution of DNA was stored at 4 °C. The interaction of **1a**, **2a**, and **2b** having three different geometries with CT-DNA was studied by dissolving each complex in 2 mL of DMSO and diluting with tris–HCl buffer to get the required concentration for all the experiments. Absorption spectral titration experiments were performed by maintaining the complex concentration constant and varying the CT-DNA concentration. To eliminate the absorbance of DNA itself, an equal amount of CT-DNA was added to the reference solution.

In the EB fluorescence displacement experiment, 5.0 μL of the EB tris–HCl solution (1.0 mmol L^{-1}) was added to 1.0 mL of DNA solution (at saturated binding levels) [27] and stored in the dark for 2.0 h. Then, the solution of the complex was titrated into the

Table 1.   Crystallographic data and details of refinement for **1b**, **2a**, and **2b**.

	$[Cu(L^1)_2](NO_3)_2$ (**1b**)	$[Cu(L^2)_2(H_2O)_2](ClO_4)_2$ (**2a**)	$[Cu(L^2)_2(H_2O)](NO_3)_2$ (**2b**)
Empirical formula	$C_{22}H_{20}CuN_6O_{10}$	$C_{22}H_{24}Cl_2CuN_4O_{12}S_2$	$C_{22}H_{24}CuN_6O_{10}S_2$
Formula weight	591.98	735.01	660.13
Crystal system	Monoclinic	Monoclinic	Triclinic
Space group	$P\,2_1/c$	$P\,2_1/n$	$P\,1$
a (Å)	9.2312(4)	8.672(4)	7.6007(4)
b (Å)	9.3425(4)	11.917(4)	9.0032(5)
c (Å)	14.4890(6)	14.220(6)	11.5900(6)
α (°)	90.0	90.0	94.009(3)
β (°)	105.625(2)	94.18(3)	107.923(3)
γ (°)	90.0	90.0	108.609(3)
Volume (Å^3)	1203.39(9)	1465.6(10)	702.63(6)
Z	2	2	1
Density (g cm^{-3})	1.634	1.665	1.560
$F(000)$	606	750	339
θ range (°)	3.19–28.35	2.91–22.53	1.88–28.38
Collected reflections	20,959	16,190	12,909
R_{int}	0.0281	0.1349	0.0205
Unique reflections	3012	1903	6649
Observed data $[I > 2.0\,\sigma(I)]$	2527	1425	5595
Goodness of fit	1.024	1.045	1.004
Parameters	181	205	390
$R1$ $[I > 2.0\,\sigma(I)]$	0.0324	0.0588	0.0406
$wR2$ $[I > 2.0\,\sigma(I)]$	0.0861	0.1595	0.1083
Residuals (e Å^{-3})	0.336, −0.430	0.669, −0.482	0.354, −0.256

DNA/EB mixture and diluted with tris–HCl buffer to 5.0 mL to get the appropriate complex/CT-DNA mole ratio in solution. Before measurements, the mixture was shaken and incubated at room temperature for 30 min. The fluorescence spectra of EB bound to DNA were obtained with an λ_{ex} of 522 nm.

To ascertain the binding mode (groove/intercalative) of the complexes with DNA, the viscosity measurement method was used by employing an Ostwald's viscometer. Titrations were carried out in the viscometer by adding the complex (0.5–3.5 μM) to the CT-DNA solution (5.0 μM). The viscosity value of the solutions was calculated from the observed flow time of CT-DNA-containing solution corrected from the flow time of buffer alone (t_0), $\eta = t - t_0$. The obtained data were used to plot the $(\eta/\eta_0)^{1/3}$ *versus* the ratio of the concentration of complex to CT-DNA, where η is the viscosity of the CT-DNA solution in the presence of complex and η_0 is the viscosity of the CT-DNA solution only.

2.7. *Theoretical calculations*

To clarify the configurations and energy levels of **1a**, **2a**, and **2b**, density functional theory (DFT) calculations were performed using Gaussian-09 software over a Red Hat Linux IBM cluster. Molecular level interactions were also studied using DFT with the B3LYP/6–31G (d, p) functional model and basis set. Vertical electronic excitations based on B3LYP optimized geometry were computed using the time-dependent density functional theory (TD-DFT) formalism in water. The conductor-like polarizable continuum model was used to calculate the fractional contributions of various groups to each molecular orbital. The lowest 20 singlet states along the vertical excitation energies are computed here.

3. Results and discussion

3.1. *Synthesis and characterization*

The carboxamide derivatives L^1 and L^2 were synthesized by reaction between pyridine-2-carboxylic acid with the proper amine (furfurylamine for L^1 or 2-thiophenemethyl amine for L^2) in pyridine (scheme 1), and the formulation of the ligands has been established using spectroscopic and physicochemical tools. Each ligand was treated with the perchlorate and nitrate copper(II) salts in ethanol which led to the formation of four mononuclear copper(II) complexes, $[Cu(L^1)_2](ClO_4)_2$ (**1a**), $[Cu(L^1)_2](NO_3)_2$ (**1b**), $[Cu(L^2)_2(H_2O)_2](ClO_4)_2$ (**2a**), and $[Cu(L^2)_2(H_2O)](NO_3)_2 \cdot H_2O$ (**2b**), which were obtained as blue microcrystalline solids upon evaporation. All the complexes are completely soluble in common organic solvents. The formulation of the complexes has been confirmed by spectroscopic methods, elemental analyses, and also by X-ray diffraction.

3.2. *Structural description of 1b, 2a, and 2b*

ORTEP views with the atom numbering scheme of **1b**, **2a**, and **2b** are illustrated in figures 1–3, respectively, and a selection of bond distances and angles are listed in table 2.

Complexes **1a** and **1b** are isostructural and both crystallize in the monoclinic system, space group $P2_1/c$. In these monomeric complexes (figures 1 and s1), the copper(II) is located on a crystallographic inversion center and is bis-chelated by two L^1 ligands through the pyridine N and carbonyl O donors in *trans* fashion, resulting in a square planar coordination. The structural data of **1a** were of low accuracy (see experimental section); the description is restricted to **1b** only. The Cu-N(1) and Cu–O(1) bond distances are 1.9758(14) and 1.9618(12) Å, respectively, with a bite angle of 82.83(5)°. The nitrates are symmetrically located at axial positions with long Cu–ONO$_2$ distances of 2.5706(17) Å (figure 1). In the crystal packing, each amino group N(2)–H is involved in a hydrogen bond with an oxygen of the nitrate (N···O distance = 2.882(2) Å, N–H···O = 166°), leading to the formation of 1-D chains (figure 4).
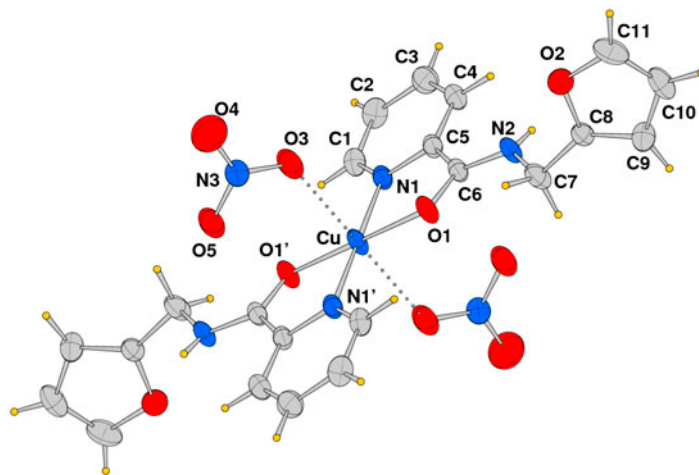

Figure 1.   ORTEP view of $[Cu(L^1)_2](NO_3)_2$ (**1b**) with label scheme of the crystallographic independent atoms.
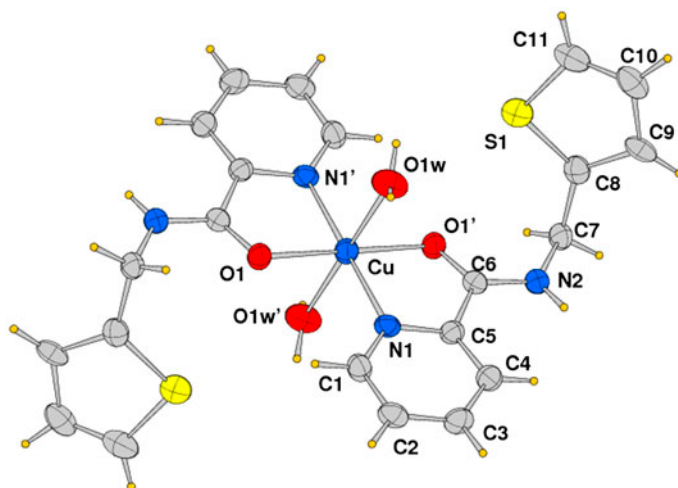
Figure 2.   ORTEP drawing of $[Cu(L^2)_2(H_2O)_2]^{2+}$ of **2a** with label scheme of the crystallographic independent atoms.

Table 2.   Coordination bond lengths (Å) and angles (°) for **1b**, **2a**, and **2b**.

1b			
Cu(1)–N(1)	1.9758(13)	Cu(1)–O(1)	1.9618(12)
O(1)–Cu(1)–N(1)	82.83(5)	N(1)–Cu(1)–N(1')	180.0
N(1)–Cu–O(1')	97.17(5)	O(1)–Cu(1)–O(1')	180.0
2a			
Cu–N(1)	1.976(4)	Cu–O(1)	1.977(4)
Cu–O(1w)	2.434(4)	N(1)–Cu–O(1w')	93.79(17)
N(1)–Cu–O(1)	82.09(16)	O(1)–Cu–O(1w')	92.54(17)
N(1)–Cu–O(1')	97.91(16)	N(1')–Cu–N(1)	180.0
N(1)–Cu–O(1w)	86.21(17)	O(1)–Cu–O(1')	180.0
O(1)–Cu–O(1w)	87.46(17)	O(1w)–Cu–O(1w')	180.0
2b			
Cu–N(1)	1.962(4)	Cu–O(1)	1.970(4)
Cu–N(3)	1.982(4)	Cu–O(2)	1.966(3)
Cu–O(1w)	2.278(6)	N(1)–Cu–N(3)	170.96(16)
N(1)–Cu–O(1)	82.25(16)	N(1)–Cu–O(1w)	94.9(2)
O(2)–Cu–N(3)	82.59(16)	O(1)–Cu–O(1w)	91.8(2)
N(1)–Cu–O(2)	96.39(15)	N(3)–Cu–O(1w)	94.1(2)
O(1)–Cu–N(3)	97.89(15)	O(2)–Cu–O(1w)	93.8(2)
O(2)–Cu–O(1)	174.39(18)		

Note: Symmetry code for primed atoms: 1-*x*, 1-*y*, 2-*z* (**1a**); 1-*x*, 1-*y*, 1-*z* (**1b**); -*x*, -*y*, 1-*z* (**2a**).

In the solid state structure of **2a** and **2b**, copper(II) is chelated by two $\mathbf{L^2}$ ligands, similar to $\mathbf{L^1}$ with the pyridine N and carbonyl O in *trans* fashion, but the complexes differ in coordination geometry, being octahedral and square pyramidal, respectively. In **2a**, two water molecules are located in the axial positions (figure 3) giving an octahedral species located on a crystallographic center of symmetry. Complex **2a** was obtained using the same copper(II) salt (hexahydrate copper(II) perchlorate) as for **1a**. The Cu–N(1) and Cu–O(1) bond distances, of 1.976(4) and 1.977(4) Å, are comparable to those measured in **1a**, while the Cu–O(1w) bond length is significantly longer (2.434(4) Å) [28] due to the Jahn–Teller
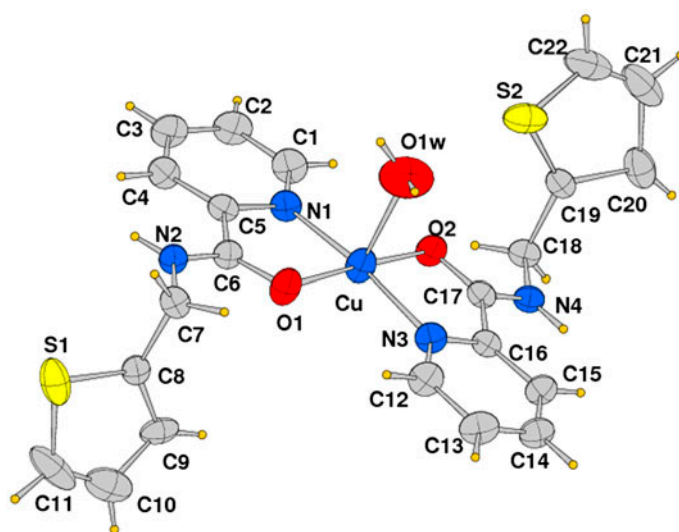
Figure 3. ORTEP drawing of $[Cu(L^2)_2(H_2O)]^{2+}$ of **2b** with atom labeling scheme.

effect, as expected. A hydrogen bond is detected between each N(2)–H group and a perchlorate oxygen (N⋯O = 2.948(6) Å, figure s2). The aqua ligands interact very weakly with perchlorate oxygens (O1w⋯O distances longer than 3.0 Å).

Complex **2b** exhibits a distorted square pyramidal geometry, comprising two chelating ligands in the basal plane and a water in the apical position of the pyramid (figure 4). The
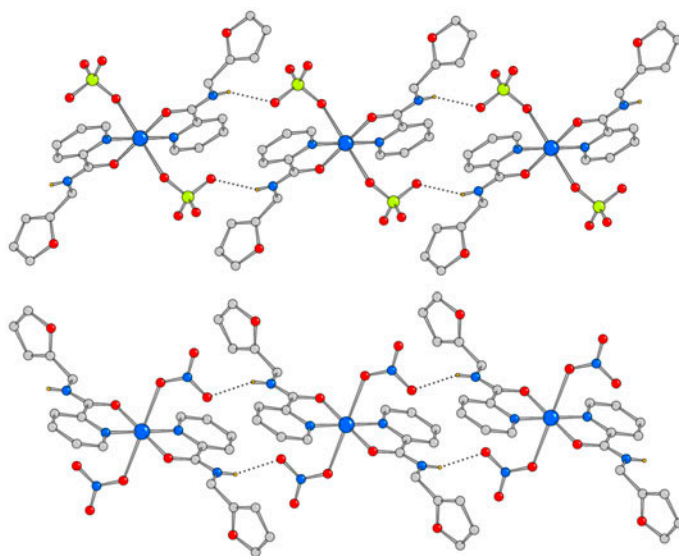

Figure 4. Crystal packing of **1a** and **1b** with indication of the 1-D chains developed along the *a* axis due to hydrogen bonding interactions involving amine N(2)–H with anion oxygens.

trigonality index [29, 30] of this structure, calculated to be 0.057 [$\tau = (\beta - \alpha)/60$; where $\beta = O(2)\text{-}Cu\text{-}O(1) = 174.39°$ and $\alpha = N(1)\text{-}Cu\text{-}N(3) = 170.96°$], confirms the almost regular SP geometry. The Cu–N and Cu–O bond distances follow the same trend (table 2) as observed for the other complexes, while the Cu–O(1w) bond length is 2.278(6) Å. In **2b**, the two five-membered chelating rings form a dihedral angle of *ca.* 12° assuming an umbrella conformation with the metal displaced from the basal coordination mean plane by 0.125(2) Å toward the apical water. A hydrogen bond is detected between N–H and nitrate oxygen (N(2)···O = 2.915(7), N(4)···O = 2.766(8) Å). In addition, coordinated and lattice water molecules are involved in H–bond interactions with the two nitrate anions leading to a 2-D layered structure (figure 5 and table 3).

All the coordination distances reported for the chelating ligands in these complexes are comparable despite the different coordination geometries and agree with those measured in similar mononuclear derivatives with 2-pyridinecarboxamide [31, 32]. The use of copper(II) nitrate as a reactant appears to favor the formation of a complex with a different coordination geometry with respect to **2a** (where perchlorate is the counter anion), but packing requirements cannot be excluded to explain this feature. In fact, reaction of N-(2-pyridyl)-carbonylaniline (**L**) with $Cu(NO_3)_2$ and $Cu(ClO_4)_2$ afforded complexes of same stoichiometry, namely $[Cu(L)_2(H_2O)_2](NO_3)_2$ and $[Cu(L)_2(H_2O)_2](ClO_4)_2$ [31].

3.3. *FTIR spectra*

In the IR spectrum of **L**[1], absorptions at 3344 and at 1660 cm^{-1} are assigned to the ν_{N-H} and to the $\nu_{C=O}$ stretches, respectively. The bands assignable to the corresponding $\nu_{C=O}$ stretch in **1a** and **1b** have been observed at lower frequency (1631 cm^{-1}) compared to free **L**[1], indicating coordination of the carbonyl oxygen to copper(II). In both **1a** and **1b**, a moderate absorption at *ca.* 3275 cm^{-1} has been attributable to ν_{N-H}, suggesting the presence of a non-coordinated N–H group. The bands at 1080 for $\nu_{ClO4(sym)}$ and 628 cm^{-1} for ν_{ClO4} $_{(asym)}$ have been observed while the peaks at *ca.* 1554 and 1381 cm^{-1} for ν_{NO3} confirm the presence of perchlorate and nitrate as counter anions in **1a** and **1b**, respectively.
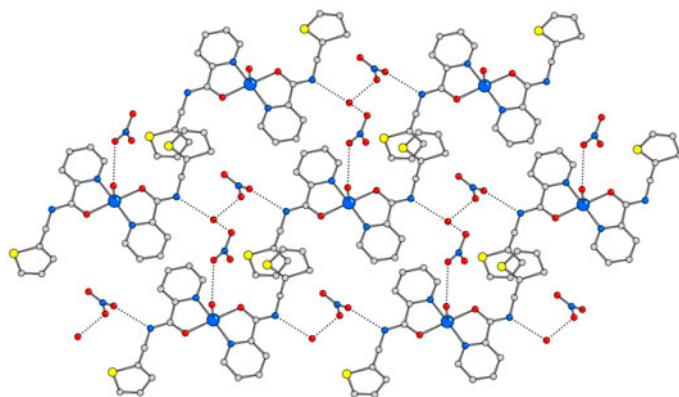

Figure 5. Crystal packing of **2b** showing the 2-D layered structure built by H–bond interactions (only those shorter than 3.0 Å are displayed).

Table 3. Geometry of hydrogen bonds (Å/°) for **2b**.

Donor–H	Acceptor	D–H	H⋯A	D⋯A	D–H⋯A	Symmetry code for A
N(2)–H(2A)	O(4)	0.89(3)	2.04(3)	2.915(7)	173(3)	$x, -1+y, z$
N(4)−H(4A)	O(2w)	0.96(7)	1.86(7)	2.766(8)	158(5)	$x, y, -1+z$
O(1w)–H(1w)	O(4)	0.84(10)	2.34(11)	3.083(10)	149(10)	–
O(1w)–H(2w)	O(7)	0.85(10)	2.58(11)	2.922(12)	105(12)	$-1+x, y, z$
O(2w)–H(21w)	O(6)	0.86(5)	1.98(5)	2.781(8)	156(12)	–
O(2w)–H(22w)	O(8)	0.87(14)	2.35(14)	2.836(11)	116(11)	$x, 1+y, 1+z$

In the IR spectrum of $\mathbf{L^2}$, absorptions at 3317 and at 1654 cm^{-1} are assigned to the ν_{N-H} and to the $\nu_{C=O}$, respectively. In spectra of **2a** and **2b**, the $\nu_{C=O}$ band is shifted to lower frequency (1631 cm^{-1}), suggesting the coordination of the carbonyl oxygen to the metal center. In both **2a** and **2b**, a moderate absorption at *ca.* 3449 cm^{-1} is assigned to ν_{O-H} of water. In addition, the bands at 1118, 1080, and 628 cm^{-1} assignable to the symmetric and asymmetric stretching of ν_{ClO4} for the perchlorate of **2a** and the sharp absorptions at 1554 and 1382 cm^{-1} for ν_{NO3} of nitrate of **2b** help to validate the formulation of the complexes.

3.4. *Electronic spectra*

The electronic spectra of **1a**, **2a**, and **2b** in ethanol are shown in figures s3 and s4, respectively, and the spectral data are tabulated in table 4. Complexes **1** and **2** displayed a lower energy band at 688, 685, 684, and 680 nm, respectively, with low extinction coefficient values that correspond to the d–d transition. Complexes **1a** and **1b** display high energy bands with high extinction coefficient at 376 and 378 nm, respectively, and are correlated with the theoretical values (381 nm) and **1a** and **1b** also show a high energy band with high extinction coefficient at 272 and 275 nm, respectively. Complexes **2a** and **2b** display high energy bands at 379 and 381 nm, respectively, with high extinction coefficient again correlated with theoretical values (380 nm).

The UV spectra computed from TDDFT calculations in water show important peaks from 350 to 450 nm. For **1a**, the band at 381 nm is dominated by the HOMO → LUMO + 2, HOMO−1 → LUMO + 1 excitation, and the band at 385 nm is dominated by the HOMO−1 → LUMO + 1 transition (figure s5). For **2a** and **2b**, the bands at 380 and 381 nm are mainly due to HOMO−1 → LUMO + 2, HOMO−1 → LUMO and HOMO−1 → LUMO, HOMO−1 → LUMO + 1 transitions, respectively (figures s6 and s7). The details of the energy state, vertical excitation energies, oscillator strengths, and salient transitions are shown in tables s3–s6. Here, the calculated spectra of the complexes are found to be compatible with the experimental ones.

Table 4. Electronic absorption spectral data in ethanol.

Complex	λ (nm) ε (dm^3 mol^{-1} cm^{-1})
1a	688 (1375), 376 (11,875), 272 (31,500)
2a	684 (2148), 379 (30,945)
2b	680 (1519), 411 (9469), 293 (1024)

3.5. *DNA-binding study of 1a* and 2

The interaction of **1a** and **2** with CT-DNA has been investigated using absorption and emission spectra. The study for **1b** was not carried out having similar structure to **1a**. To examine the binding mode of metal complexes with DNA, electronic absorption spectroscopy is used as a characterization tool. In general, binding of the metal complex to the DNA helix is shown by an increase of the n → π* band of the copper(II) complex due to the involvement of strong intercalative interactions between the effective chromophore of the complexes and the base pairs of DNA [33–35]. The absorption spectra of **1a**, **2a**, and **2b** in the absence and presence of increasing amounts DNA (at a constant concentration of complexes) are given in figures 6, s8, and s12. The extent of the hyperchromism in the absorption band is generally consistent with the strength of intercalative interaction [36–39], and the observed spectral changes indicate a strong interaction of the copper(II) complexes with CT-DNA.

In order to establish the binding strength of the metal complexes with CT-DNA, the apparent association constant K_b was determined from the spectral titration data using the following equation [40]:

$$[DNA]/(\varepsilon_a - \varepsilon_f) = [DNA]/(\varepsilon_b - \varepsilon_f) + 1/[K_b(\varepsilon_b - \varepsilon_f)]$$

where [DNA] is the concentration of DNA, ε_f, ε_a, and ε_b correspond to the extinction coefficients for the free complex, for each addition of DNA to the copper(II) complex and for the copper(II) complex in the fully bound form, respectively. Plots of $[DNA]/(\varepsilon_a-\varepsilon_f)$ *versus* [DNA] (figures 7, s9, and s13) gave the apparent association constant K_b as the ratio of the slope to the intercept. The binding constants K_b for **1a**, **2a**, and **2b** were 2.44×10^5 M^{-1} (R = 0.94178, $n = 5$ points), 1.13×10^4 M^{-1} (R = 0.95755, $n = 4$ points), and 3.94×10^4 M^{-1} (R = 0.98489, $n = 5$ points), respectively, which are significantly greater compared to free **L^1** and **L^2** as the corresponding K_b values are 8.29×10^3 for **L^1** and 7.63×10^3 M^{-1} for **L^2**. The K_b values suggest that **1a**, **2a**, and **2b** bind DNA in intercalative mode involving a good stacking interaction of the furan or thiophene chromophore with
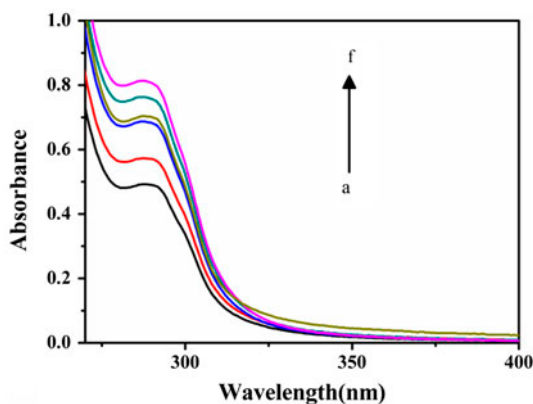

Figure 6.   Electronic spectral titration of **1a** with CT-DNA in tris–HCl buffer at 288 nm; [complex] = 2.42×10^{-5}; [DNA]: (a) 0.0. (b) 1.75×10^{-6}. (c) 3.6×10^{-6}. (d) 4.8×10^{-6}. (e) 6.14×10^{-6}. (f) 7.80×10^{-6} mol L^{-1}.
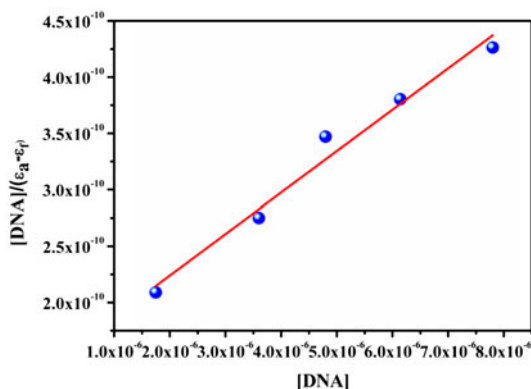Note: The arrow denotes the gradual increase of DNA concentration.

Figure 7.　Plot of $[DNA]/(\varepsilon_a - \varepsilon_f)$ *vs.* [DNA] for the absorption titration of CT-DNA with **1a** in tris–HCl buffer; association constant K_b: 2.44×10^5 M^{-1} for ($R = 0.9716$, $n = 5$ points).

the base pairs of DNA. The K_b of **1a** is comparable with the values of the previously reported copper(II) complexes, [46, 47] but higher than those reported [48–52] and those of **2**, indicating that **1a** binds DNA by intercalation more strongly than **2a** and **2b**.

The propensity of the complexes to interact with CT-DNA has been analyzed by the fluorescence spectral technique using the emission intensity of EB. Although EB does not show any emission in the buffer medium due to fluorescence quenching by solvent, it shows an emission band in the presence of CT-DNA due to intercalative binding to the helix. The fluorescence intensity of the DNA-bound EB (with an excitation wavelength of 522 nm) decreases with increasing concentration of the complexes (see figures 8, s10, and s14). This is observed since the binding of copper(II) complexes to DNA promotes the release of EB molecules from the helix and leading to a concomitant decrease in the fluorescence
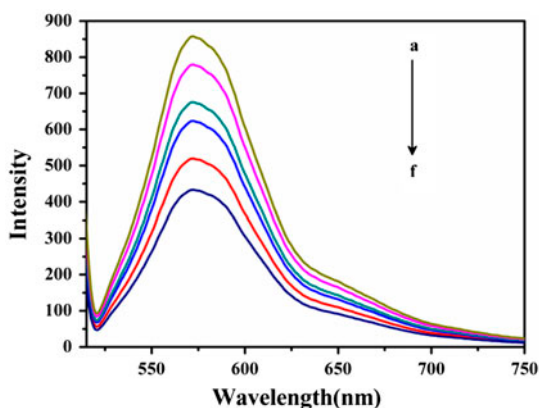

Figure 8.　Emission spectra of the CT-DNA-EB system in tris–HCl buffer upon titration with **1a**. $\lambda_{ex} = 522$ nm; [EB] = 1.79×10^{-6} mol L^{-1}, [DNA] = 1.23×10^{-5}; [Complex]: (a) 0.0. (b) 1.81×10^{-6}. (c) 2.36×10^{-6}. (d) 3.60×10^{-6}. (e) 4.72×10^{-6}. (f) 6.34×10^{-6} mol L^{-1}. The arrow denotes the gradual increase of complex concentration.

emission [41]. This quenching due to the addition of the metal complexes is in agreement with the linear Stern–Volmer equation [42]:

$$I_0/I = 1 + K_{sv}[Q]$$

where I_0 and I represent the fluorescence intensities in the absence and presence of quencher, respectively. K_{sv} is the linear Stern–Volmer quenching constant and Q denotes the concentration of the quencher. In the plot (see figures 9, s11, and s15) of I_0/I *versus* [complex], K_{sv} value is given by the slope of the regression line. The K_{sv} values are 2.45×10^5, 0.87×10^4, and 8.51×10^4 for **1a**, **2a**, and **2b**, respectively, suggesting a strong affinity of each metal complex to CT-DNA (table 5).

   The interactions between the complexes and DNA were investigated by viscosity measurement, which is regarded as the most effective method to study intercalative binding mode of DNA in solution [43, 44]. A classical intercalative mode causes a significant increase in viscosity of the DNA solution due to an increase in the separation of base pairs at the intercalation sites and hence an increase in overall DNA length. In contrast, a partial, non-classical intercalation of ligand could bend (or kink) the DNA helix, thus reducing its effective length and concomitantly its viscosity [45]. As seen in figure 10, the viscosity of CT-DNA increases with the increase in the ratio of **1a**, **2a**, and **2b** to CT-DNA.

3.6. *Redox behavior*

The electrochemical properties for **1a** and **2** have been studied by cyclic voltammetry in dry DMF and in the presence of [Bu$_4$N]ClO$_4$ as supporting electrolyte at room temperature. Three electrode cell setup such as platinum, Ag/AgCl, and a platinum wire as a working, reference and auxiliary electrode, respectively, have been used for measurements. The cyclic voltammograms of **1a** and **2** are displayed in figures 11, s16, and s17, respectively; the electrochemical data have been tabulated in table 6. The complexes exhibit a quasi-reversible voltammogram in the range of $E_{1/2}$ value from ≈ -0.80 to -0.915 V
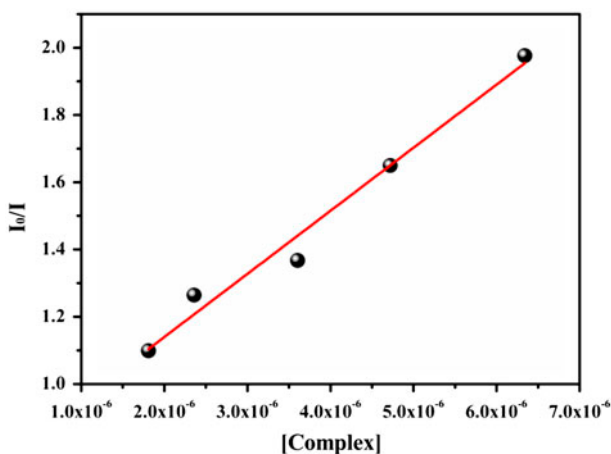

Figure 9.   Plot of I_0/I *vs*. [complex] of **1a**; $K_{sv} = 2.45 \times 10^5$ ($R = 0.9745$, $n = 5$ points).

Table 5. K_b and K_{SV} values of DNA-binding study.

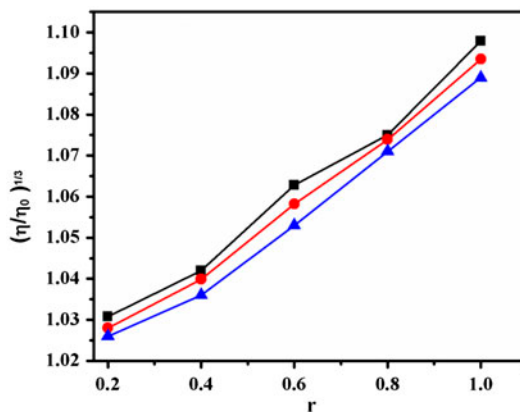| Complex	K_b	K_{SV}
1a	2.44×10^5	2.45×10^5
2a	1.13×10^4	0.87×10^4
2b	3.94×10^4	8.51×10^4

Figure 10. Change in the relative viscosity $(\eta/\eta_0)^{1/3}$ of CT-DNA as a function of r, the molar ratio of the compound to the DNA base pairs. The effect of increasing amounts of the concentration of **1a** (■), **2a** (●), and **2b** (▲) on the relative viscosities of CT-DNA.
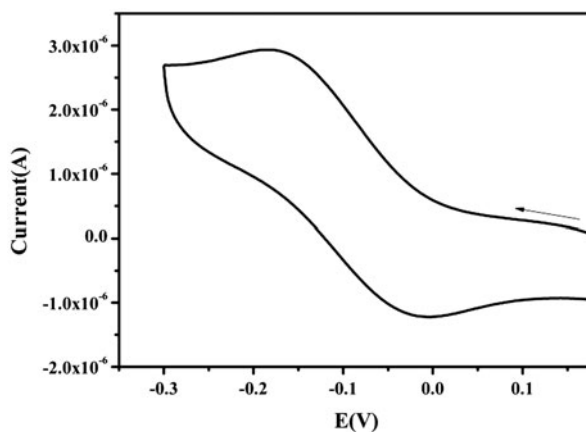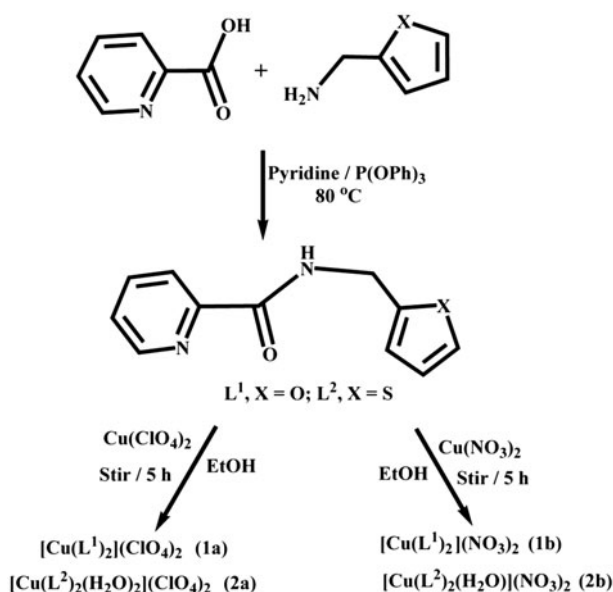

Figure 11. Cyclic voltammogram (scan rate 50 mV/s) of $[Cu(L^1)_2](ClO_4)_2$ (**1a**) in DMF.

(*versus* Ag/AgCl) corresponding to the Cu^{2+}/Cu^+ redox couple. The trend of reduction potential values in the order **1a** (−80 mV) < **2b** (−96 mV) < **2a** (−103 mV) can be explained by the geometry and the coordination number of copper(II) and is further

Scheme 1. Synthetic procedure of the ligands and their corresponding complexes in ethanol.

Table 6. Electrochemical data for **1a**, **2a**, and **2b** in DMF.

Complex	E_{pc} (mV)	E_{pa} (mV)	ΔE_p (mV)	$E_{1/2}$ (mV)
1a	−170	−10	160	−80
2a	−193	13	206	−103
2b	−176	16	192	−96

supported by theoretical calculations obtained from DFT study (*viz.* Supporting Information) since LUMO of **1a** is at the lowest energy (−3.15 eV) and that of **2a** at the highest (−2.72 eV) among these complexes.

4. Conclusion

Syntheses and characterizations of four new mononuclear copper(II) complexes of two newly designed carboxamide derivatives L^1 and L^2 have been reported. While reactions of L^1 with copper perchlorate and nitrate give four-coordinate mononuclear copper(II) complexes, $[Cu(L^1)_2](ClO_4)_2$ (**1a**) and $[Cu(L^1)_2](NO_3)_2$ (**1b**), the reactions of L^2 with same metal salts give six- and five-coordinate mononuclear species, $[Cu(L^2)_2(H_2O)_2](ClO_4)_2$ (**2a**) and $[Cu(L^2)_2(H_2O)](H_2O)(NO_3)_2$ (**2b**), respectively. Thus, the coordination geometry of the complexes is affected by the chelating ligands, although these have non-coordinating heterocycle rings of the same bulk (furan in L^1 and thiophene in L^2) in the structure. In addition, the interaction of the complexes to CT-DNA, investigated by electronic absorption

titrations, fluorescence spectroscopy, and viscosity measurements, indicates that square planar complex **1a** interacts with CT-DNA in intercalative mode more strongly than the octahedral (**2a**) and the square pyramidal (**2b**) derivative.

Supplementary material

Crystallographic data for the structural analyses of the complexes have been deposited with the Cambridge Crystallographic Data Center, CCDC Nos. 1029484-1029486 for **1a**, **2a** and **2b**, respectively, and CCDC No. 1056581 for **1b**. Copies of this information are available on request free of charge from CCDC, 12 Union Road, Cambridge, CB21EZ, UK (Fax: +44 1223 336-033; E mail: deposit@ccdc.ac.uk or http://www.ccdc.cam.ac.uk).

Acknowledgements

Disclosure statement

No potential conflict of interest was reported by the authors.

References

[1] J. Lin, J.Y. Zhang, Y. Xu, X.K. Ke, Z. Guo. *Acta Crystallogr., Sect. C: Cryst. Struct. Commun.*, **57**, 192 (2001).
[2] B.M. Trost, I. Hachiya. *J. Am. Chem. Soc.*, **120**, 1104 (1998).
[3] J.D. Epperson, L.J. Ming, G.R. Baker, G.R. Newkome. *J. Am. Chem. Soc.*, **123**, 8583 (2001).
[4] S.R. Collinson, T. Gelbrich, M.B. Hursthouse, J.H.R. Tucker. *Chem. Commun.*, 555 (2001).
[5] J. Zhang, Q. Liu, C. Duan, Y. Shao, J. Ding, Z. Miao, X. You, Z. Guo. *J. Chem. Soc., Dalton Trans.*, **22**, 591 (2002).
[6] J. Li, M.L. Zheng, I. King, T.W. Doyle, S.H. Chen. *Curr. Med. Chem.*, **8**, 121 (2001).
[7] X.M. He, D.C. Carter. *Nature*, **358**, 209 (1992).
[8] T. Mukherjee, B. Sen, E. Zangrando, G. Hundal, B. Chattopadhyay, P. Chattopadhyay. *Inorg. Chim. Acta*, **406**, 176 (2013) and references therein.
[9] J.A. Cowan. *Curr. Opin. Chem. Biol.*, **5**, 634 (2001).
[10] S. Dhar, D. Senapati, P.K. Das, P. Chattopadhyay, M. Nethaji, A.R. Chakravarty. *J. Am. Chem. Soc.*, **125**, 12118 (2003).
[11] Y. Li, Y. Wu, J. Zhao, P. Yang. *J. Inorg. Biochem.*, **101**, 283 (2007).
[12] N.S. Devi, L.J. Singh, S.P. Devi, R.K.B. Singh, R.K.H. Singh, B. Rajeswari, R.M. Kadam. *J. Mol. Struct.*, **1076**, 411 (2014).
[13] X. Sheng, X. Guo, X.M. Lu, G.Y. Lu, Y. Shao, F. Liu, Q. Xu. *Bioconjugate Chem.*, **19**, 490 (2008) and references therein.
[14] X.W. Li, L. Tao, Y.T. Li. *Eur. J. Med. Chem.*, **54**, 697 (2012).
[15] S. Sarkar, T. Mukherjee, S. Sen, E. Zangrando, P. Chattopadhyay. *J. Mol. Struct.*, **980**, 117 (2010).
[16] F.H. He, L. Tao, X.W. Li, Y.T. Li. *New J. Chem.*, **36**, 2078 (2012).
[17] A. Patra, T. Mukherjee, S. Sarkar, E. Zangrando, P. Chattopadhyay. *Polyhedron*, **30**, 2783 (2011).
[18] S. Dey, S. Sarkar, T. Mukherjee, B. Mondal, E. Zangrando, J.P. Sutter, P. Chattopadhyay. *Inorg. Chim. Acta*, **376**, 129 (2011).
[19] S. Dey, S. Sarkar, H.S. Evans, P. Chattopadhyay. *Transition Met. Chem.*, **36**, 631 (2011).
[20] S. Sarkar, S. Sen, S. Dey, E. Zangrando, P. Chattopadhyay. *Polyhedron*, **29**, 3157 (2010).
[21] S. Dey, S. Sarkar, H. Paul, E. Zangrando, P. Chattopadhyay. *Polyhedron*, **29**, 1583 (2010).

[22] Bruker. *SMART, SAINT. Software Reference Manual*, Bruker AXS Inc., Madison, WI (2000).
[23] G.M. Sheldrick. *Acta Crystallogr. Sect. A: Found. Crystallogr.*, **64**, 112 (2008).
[24] L.J. Farrugia. *J. Appl. Crystallogr.*, **32**, 837 (1999).
[25] J. Marmur. *J. Mol. Biol.*, **3**, 208 (1961).
[26] M.E. Reichmann, S.A. Rice, C.A. Thomas, P. Doty. *J. Am. Chem. Soc.*, **76**, 3047 (1954).
[27] J.K. Barton, J.M. Goldberg, C.V. Kumar, N.J. Turro. *J. Am. Chem. Soc.*, **108**, 2081 (1986).
[28] B.H. Chen, H.H. Yao, W.T. Huang, P. Chattopadhyay, J.M. Lo, T.H. Lu. *Solid State Sci.*, **1**, 119 (1999).
[29] A.W. Addison, T.N. Rao, J. Reedijk, J. van Rijn, G.C. Verschoor. *J. Chem. Soc., Dalton Trans.*, 1349 (1984).
[30] P.K. Dhara, S. Pramanik, T.H. Lu, M.G.B. Drew, P. Chattopadhyay. *Polyhedron*, **232**, 457 (2004).
[31] F. Lebon, M. Ledecq, M. Dieu, C. Demazy, J. Remacle, R. Lapouyade, O. Kahn, F. Durant. *J. Inorg. Biochem.*, **86**, 547 (2001).
[32] A. Morsali, A. Ramazani, A.R. Mahjoub. *J. Coord. Chem.*, **56**, 1555 (2003).
[33] J. Sun, S. Shuo, Y. An, J. Liu, F. Gao, L.N. Ji, Z.W. Mao. *Polyhedron*, **27**, 2846 (2008).
[34] V. Lombardo, R. Bonomi, C. Sissi, F. Mancin. *Tetrahedron*, **66**, 2189 (2010).
[35] K. Dhara, J. Ratha, M. Manassero, X.Y. Wang, S. Gao, P. Banerjee. *J. Inorg. Biochem.*, **101**, 95 (2007).
[36] K. Dhara, P. Roy, J. Ratha, M. Manassero, P. Banerjee. *Polyhedron*, **26**, 4509 (2007).
[37] V.A. Bloomfield, D.M. Crothers, I. Tinoco. *Phys. Chem. Nucl. Acids*, Harper and Row, New York, NY 432–434 (1974).
[38] S.A. Tysoe, R.J. Morgan, A.D. Baker, T.C. Strekas. *J. Phys. Chem.*, **97**, 1707 (1993).
[39] J.K. Barton, A.T. Danishefsky, J. Goldberg. *J. Am. Chem. Soc.*, **106**, 2172 (1984).
[40] J.M. Kelly, A.B. Tossi, D.J. McConnell, C. OhUigin. *Nucl. Acid. Res.*, **13**, 6017 (1985).
[41] R. Vijayalakshmi, M. Kanthimathi, V. Subramanian, B.U. Nair. *Biochem. Biophys. Acta*, **1475**, 157 (2000).
[42] O. Stern, M. Volmer. *Z. Phys.*, **20**, 183 (1919).
[43] J. Ravichandran, P. Gurumoorthy, M.A. Imran Musthafa, A. Kalilur Rahiman. *Spectrochim. Acta, Part. A*, 133, 785 (2014).
[44] N.S. Devi, L.J. Singh, S.P. Devi, R.K.B. Singh, R.K.H. Singh, B. Rajeswari, R.M. Kadam. *J. Mol. Struct.*, **1076**, 411 (2014).
[45] A. Kathiravan, R. Renganathan. *Polyhedron*, **28**, 1374 (2009).
[46] J.-L. Li, L. Jiang, S.-T. Li, J.-L. Tian, W. Gu, X. Liu, S.-P. Yan. *J. Coord. Chem.*, **67**, 3598 (2014).
[47] L. Subha, C. Balakrishnan, S. Thalamuthu, M.A. Neelakantan. *J. Coord. Chem.*, **68**, 1021 (2015).
[48] R.K.B. Devi, S.P. Devi, R.K.B. Singh, R.K.H. Singh, T. Swu, W.R. Devi, C.H.B. Singh. *J. Coord. Chem.*, **67**, 891 (2014).
[49] M. Iqbal, S. Ali, Z.-U. Rehman, N. Muhammad, M. Sohail, V. Pandarinathan. *J. Coord. Chem.*, **67**, 1731 (2014).
[50] R.-R. Duan, L. Wang, W.-Q. Huo, S. Chen, X.-H. Zhou. *J. Coord. Chem.*, **67**, 2765 (2014).
[51] M. Nandy, D.L. Hughes, G.M. Rosair, R.K.B. Singh, S. Mitra. *J. Coord. Chem.*, **67**, 3335 (2014).
[52] X.-J. Li, K. Zheng, Y.-T. LI, C.-W. Yan, Z.-Y. Wu, S.-Y. Xuan. *J. Coord. Chem.*, **67**, 928 (2014).